Available online at www.sciencedirect.com
ScienceDirect
Journal of Catalysis 251 (2007) 258–270
JOURNAL OF CATALYSIS
www.elsevier.com/locate/jcat

Surface modification of nano-sized HZSM-5 and HFER by pre-coking and silanization

F. Bauer [a,*], W.H. Chen [b], E. Bilz [a], A. Freyer [a], V. Sauerland [c], S.B. Liu [b,*]

[a] *Leibniz-Institut für Oberflächenmodifizierung, Permoserstr. 15, D-04318 Leipzig, Germany*
[b] *Institute of Atomic and Molecular Sciences, Academia Sinica, P.O. Box 23-166, Taipei, Taiwan 106, ROC*
[c] *Bruker Daltonik GmbH, Fahrenheitstr. 4, D-28359 Bremen, Germany*

Received 5 July 2007; revised 2 August 2007; accepted 11 August 2007

Available online 19 September 2007

Abstract

Deposition of carbonaceous and siliceous materials was used to enhance the selectivity of HZSM-5 and HFER by passivating non-selective acid sites present on the external surface of zeolite crystallites. The nature of carbonaceous deposits formed during the pre-coking treatment was studied by matrix-assisted laser desorption/ionization time-of-flight mass spectrometry (MALDI-TOF MS) after zeolite dissolution by hydrofluoric acid. Molecular weights up to 1300 Da were observed for coke species present on the pre-coked HZSM-5 sample to which carbon numbers $n_C \sim 100$ can be assigned. In terms of inactivation of surface acidity, samples modified by pre-coking were found to be more effective compared to those by one-cycle silica deposition, as evidenced by ^{31}P MAS NMR of adsorbed tributylphosphine oxide as the probe molecule. Accordingly, pre-coked HZSM-5 yielded a higher shape selectivity during xylene isomerization, i.e., a reduced formation of undesirable toluene and trimethylbenzenes. For skeletal isomerization of *n*-butene on HFER, silanization caused a decrease in isobutene formation due to the deposition of siliceous materials within the channels. Pre-coking of HFER showed no specific effect on isobutene selectivity and, accordingly, these polyaromatic carbonaceous deposits cannot be assigned to specific catalytic sites.
© 2007 Elsevier Inc. All rights reserved.

Keywords: Zeolites; Surface modification; Pre-coking; Silanization; Coke characterization; MALDI-TOF MS; Xylene isomerization; *n*-Butene isomerization

1. Introduction

Because of their ideal pore size and high catalytic activity, aluminosilicate zeolites are of enormous commercial importance for the production of hydrocarbons. For example, HZSM-5 and HFER reveal an excellent selectivity as catalysts for the isomerization of xylenes [1,2] and the skeletal isomerization of *n*-butene [3], respectively. However, the transport of molecules through the zeolite crystallites often limits the efficiency of catalytic processes. To reduce the transport resistance and the diffusion path length, nano-sized zeolite crystallites can be applied facilitating the accessibility of molecules to the internal zeolite surface and improving their catalytic performance. Although the reaction rate may be increased by using zeolites with smaller crystallite sizes, their large external surface (in comparison to micron-sized zeolites) may also provoke undesired non-selective surface reactions such as transalkylation of xylenes or secondary isomerization steps of isobutene formed. Thus, surface modification, i.e., inactivation of external catalytic sites, is crucial for fine-tuning the shape selective and catalytic properties of nano-sized zeolites. Various surface modification methods, e.g., impregnation of metal oxides [4,5], coke-induced selectivation [6–8], and deposition of inert silica via degradation of organosilicon compounds [7,9–14], have been applied to enhance the selectivity of zeolites in hydrocarbon processing. In general, the modifications should substantially suppress undesired reactions occurring on the external surface and/or decrease the diffusivity of undesired reactants in or out of the zeolite pores.

For the deposition of silica onto the external surface of zeolite crystallites, bulky organosilicon compounds, such as tetraethoxysilane (TEOS) and hexamethyldisilazane, are com-

* Corresponding authors. Faxes: +49 341 2353400, +886 2 23620200.
E-mail addresses: fbauer@rz.uni-leipzig.de (F. Bauer), sbliu@sinica.edu.tw (S.B. Liu).

0021-9517/$ – see front matter © 2007 Elsevier Inc. All rights reserved.
doi:10.1016/j.jcat.2007.08.009

monly used as silanizing agents. Whereas the postsynthetic modification of HZSM-5 by the deposition of silica on the external surface has proven to be an effective approach for preparing highly selective catalysts for xylene isomerization [15], alkylation of toluene with methanol [7,16], and toluene disproportionation [17], the deposition of carbonaceous residues for enhancing the selectivity of zeolites has been investigate in detail by only a few workers [8,18–21]. Controlled pre-coking treatment, i.e., degradation of organic compounds at elevated temperatures prior to the normal operation run, has been found to enhance the *para*-xylene selectivity during toluene disproportionation over HZSM-5 [18]. For *m*-xylene transformation over MCM-22, Laforge et al. [14] applied various catalyst modification techniques. Pre-coking through *n*-heptane cracking, however, was not found to deactivate the external acid sites selectively. Similar findings of ineffective pre-coking were obtained by Cejka et al. [7] who concluded for toluene alkylation with methanol over HZSM-5 that pre-coke deposits affected negatively the zeolite *para*-selectivity as well as that secondary isomerization reaction of xylenes on the external surface played a minor role. On the other hand, Guisnet et al. [20] attributed the high isobutene yield to the presence of coke species during skeletal isomerization of *n*-butene over HFER. Hence, a detailed understanding of the nature, location and formation of carbonaceous deposits is crucial for further improvement of coke selectivation.

Conventional methods for coke characterization normally invoke elementary analysis, thermogravimetry, and spectroscopic techniques, e.g., $^{1}H/^{13}C$ NMR, IR, and Raman spectroscopy [22]. These methods can be further categorized into non-destructive or destructive procedures. For the latter, Guisnet and Magnoux [23] demonstrated that the release of carbonaceous residues from the zeolite framework can be achieved by first dissolving the spent zeolite catalyst in aqueous hydrofluoric acid and subsequent extracting the coke species with organic solvents such as methylene chloride. Finally, the CH_2Cl_2-soluble carbonaceous residues can be excellently characterized by GC/MS technique. For example, polyalkylated benzene and alkylated pyrene derivatives having molecular weights up to 250 $g\,mol^{-1}$ were identified on spent HZSM-5 [23]. However, the dissolution/extraction method can suffer from the drawbacks of possibly alternating the nature of carbonaceous deposits and in most cases of being unable to extract the coke species fully. It has been found that the percentage of CH_2Cl_2-soluble residues decreases with increasing reaction temperature and coke amount [24]. CH_2Cl_2-insoluble coke species were typically formed at reaction temperature of >700 K and defy an identification by GC/MS. For such CH_2Cl_2-insoluble coke species formed during methanol conversion on HZSM-5 at 693 K, ^{13}C MAS NMR spectroscopy revealed a quite similar chemical nature as observed before zeolite dissolution [25]. Cerqueira et al. [26] assumed molecular weights of about 600 $g\,mol^{-1}$ for CH_2Cl_2-insoluble coke formed during *m*-xylene transformation on HUSY at 723 K.

A preferential way to characterize the CH_2Cl_2-insoluble carbonaceous deposits is by matrix-assisted laser desorption/ionization time-of-flight mass spectrometry (MALDI-TOF MS); an efficient and reliable characterization technique that has been demonstrated in the field of polymer analysis [27]. In brief, MALDI-TOF MS utilizes a laser beam as energy source for desorbing and ionizing the sample molecules, which are subsequently analyzed by time-of-flight mass spectrometry. The primary advantage of such laser desorption/ionization scheme is the relatively low input power absorbed primarily by the matrix, which minimizes fragmentation of the analyte molecules. Thus, the obtained mass spectrum directly reflects the molecular weight of individual species as well as the molecular weight distribution of the analyzed mixture. Similarly, the experiment can also be carried out in absence of a matrix (termed as LDI-TOF MS). Both MALDI-TOF and LDI-TOF mass spectrometries are capable of providing qualitative information of the repeat units and the end groups of polymeric species [28].

For carbonaceous deposits formed during isobutane/butene alkylation over ion-exchanged (La, H)-X zeolite between 303 and 403 K, Feller et al. [29] applied MALDI-TOF MS technique to analyze the deactivated catalysts and carbonaceous residues after zeolite dissolution. They obtained a mass spectrum with a distribution of molecular weights spanning from 150 to 450 Da (corresponding to a distribution of carbon number in the range of C_{12}–C_{35} with a maximum at about C_{20}) and a repetitive pattern of 14 Da (CH_2 group). Molecular species originated from series such as C_nH_{2n-14} and C_nH_{2n-18} were found to be responsible for the observed main peaks; in good agreement with the distribution measured by GC–MS. After zeolite dissolution, the mass spectrum of the 'free' carbonaceous deposits also resembles the spectrum of the deactivated catalyst with masses corresponding to that of C_nH_{2n-22} and C_nH_{2n-24}. Moreover, MALDI-TOF MS for the spent zeolite without dissolving the zeolite allows to characterize carbonaceous residues deposited on the surface of the particles [30,31].

In this study, the physical and acidic properties of HZSM-5 and HFER zeolites before and after surface modification by pre-coking and silanization treatments have been investigated by various characterization techniques, viz. N_2 adsorption/desorption measurement, ^{129}Xe and ^{31}P NMR of adsorbed probe molecules. In particular, the nature of coke species on the pre-coked HZSM-5 sample was identified by MALDI-TOF MS technique. Furthermore, the effects of pre-coking and silanization on selectivity during xylene isomerization over HZSM-5 as well as on isobutene selectivity during skeletal isomerization of *n*-butene over HFER have also been examined.

2. Experimental

2.1. Materials

NH_4ZSM-5 ($SiO_2/Al_2O_3 = 25$) and NH_4FER ($SiO_2/Al_2O_3 = 20$) zeolites were obtained from TRICAT Zeolites GmbH and ZEOLYST Inc., respectively. Their particle sizes were found to fall between 100 and 500 nm, as revealed by scanning electron microscopy. The H-form zeolites, namely HZSM-5 and HFER, were obtained by calcining the parent commercial samples in air at 823 K.

2.2. Pre-coking and silanization procedures

To avoid any interference with carbonaceous residues formed during xylene isomerization on HZSM-5 and *n*-butene skeletal isomerization on HFER, coke deposits from methanol conversion were used as pre-coke species on both nano-sized zeolites under study. After loading with methanol vapor at room temperature for 12 h, pre-coking of HZSM-5 and HFER were performed in N_2 under static conditions at 723 K for 2 h. Subsequently, these pre-coked samples were further subjected to a coke modification treatment with H_2 at 773 K for 24 h [32]. The final coke content of both zeolites was about 0.5 wt% as determined by thermogravimetric and elementary analysis.

Silanization treatments of HZSM-5 and HFER were carried out by chemical liquid deposition of TEOS while suspending the zeolites in acetone. For each run, silane hydrolysis was accelerate and accomplished by adding the stoichiometric amount of water acidified by maleic acid. The slurry was refluxed for 1 h. After the withdrawn of acetone, the sample was calcined by heating to 823 K. As the result, the silanized zeolites were found to possess a SiO_2 coverage of about 4 wt%.

2.3. Characterization of catalysts and catalytic reaction

The BET surface area and porosity of the parent and modified zeolite samples were determined by N_2 adsorption/desorption measurements (Micromeritics ASAP 2000) at 77 K. In addition, variations in their intracrystalline porous properties were also monitored by room temperature Xe adsorption isotherms and ^{129}Xe NMR measurements [33]. ^{129}Xe NMR spectra were obtained using a Bruker MSL-300P spectrometer operating at a Larmor frequency of 83.012 MHz. Diluted xenon gas was used as the chemical shift reference. On the other hand, variations in their acid features on the external surface of the catalysts before and after surface modification treatments by pre-coking and silanization were followed by ^{31}P MAS NMR of adsorbed tributylphosphine oxide (TBPO) probe molecules [8,33]. ^{31}P MAS NMR experiments were carried out on a Bruker MSL-500P spectrometer operating at a Larmor frequency of 202.46 MHz and typically under a sample spinning rate of 10–12 kHz. Detailed description of the related experiments can be found elsewhere [34,35].

Temperature-programmed desorption (TPD) of NH_3 was recorded on a fixed-bed apparatus attached to a Sensorlab 200 D (Fisons Instruments) quadruple mass spectrometer. The sample was activated in flowing nitrogen at 773 K, loaded in flowing He with NH_3 at 373 K and subsequently purged with He at the same temperature. Finally, the TPD profiles were obtained in flowing He from 373 to 673 K at a heating rate of 10 K/min.

Pre-coked zeolites were characterized by elementary analysis (Variomax CHN, Elementar Analysensysteme GmbH) and temperature-programmed oxidation (TPO) performed on a TGA 7 thermobalance (Perkin–Elmer). Furthermore, MALDI-TOF mass spectrometry was used to obtain the molecular weight distribution of carbonaceous deposits formed during the pre-coking procedure at 773 K. For this analytical study, the deposits have been liberated from the zeolite framework by complete dissolution of pre-coked zeolites in a 40% hydrofluoric acid solution at room temperature [23]. Subsequently, the soluble coke components were extracted by CH_2Cl_2 for GC–MS measurements whereas the 'insoluble coke' remained in form of black particles. These particles were suspended in tetrahydrofuran (THF) by sonication and mixed with a solution of Dithranol as MALDI matrix (20 g L^{-1} in THF). About 0.1 μL of this mixture was hand spotted onto the stainless steel target. MS was performed on a Bruker Biflex III mass spectrometer in the reflectron mode using pulsed ion extraction. Ions were generated by a 337-nm-wavelength nitrogen laser operated under threshold conditions, i.e., the laser intensity was increased until ion signals showed up. Calibration of the mass scale was performed with spectra of poly(methyl methacrylate) standards (Polymer Standards Service GmbH) recorded under identical conditions. The same instrument was also used for laser desorption/ionization (LDI)-TOF MS experiments, only that the released coke deposits were spotted onto the target without the matrix. The LDI experiments were conducted using the same settings as in the MALDI measurements.

For catalytic experiments, samples of the parent and modified HZSM-5 and HFER were pressed into pellets. The pellets were crushed and granules of 0.3–0.6 mm were separated. Diluted with quartz, the catalyst granules of about 0.2 g were loaded into a 10-mm-diameter quartz reactor. For the application of modified HZSM-5, the catalytic performance of xylene isomerization was studied converting an industrial xylene feedstock (10 wt% ethylbenzene, 10 wt% *p*-xylene, 20 wt% *o*-xylene, and 60 wt% *m*-xylene) at 673 K and atmospheric pressure. Reaction products were analyzed on a GC (Perkin–Elmer Auto System XL) with a 15.2 m × 0.51 mm i.d. Bentone 34/Didecylphthalate SCOT column (Supelco) with a stepping temperature of 10 K/min starting from 343 K (retained for 20 min) to 373 K (retained for 40 min).

On the HFER samples, catalytic studies with a reactant stream of 5% *n*-butene in nitrogen as a balancing gas were conducted at 500–775 K and a weight hour space velocity (WHSV) of 9 g/(g_{cat} h). Reaction products were analyzed on an Al_2O_3 PLOT column (30 m × ID 0.53 mm) with a temperature program of 8 K/min starting from 313 K (retained for 3 min) to 443 K (retained for 5 min).

3. Results and discussion

Post-synthesis modification of zeolites is typically anticipated to enhance their shape selectivity. Increased shape selectivity generally points to a decrease of unselective catalytic sites. In addition to effective passivation of unselective catalytic sites, the enhancement of *para*-selectivity during transformation of aromatics requires the narrowing of pore entrances of the zeolite. However, pore narrowing is closely connected with reduced reaction rates and deemed to be undesirable for industrial applications.

For nano-sized zeolites, secondary reactions taking place on the external crystallite surface without any steric constraints can diminish the original selectivity imposed by the zeolitic channel systems. In this context, inactivation of external active sites

Table 1
Physical properties of HZSM-5 and HFER samples before and after surface modification treatments (normalized based on the content of zeolite)

HZSM-5	Parent	Pre-coked	Silanized
BET surface area (m^2/g)	311	289	296
Micropore volume (mL/g)	0.151	0.137	0.147
HFER	Parent	Pre-coked	Silanized
BET surface area (m^2/g)	266	241	253
Micropore volume (mL/g)	0.138	0.125	0.131

by pre-coking or silanization is a suitable strategic exercise to fine-tune the catalytic performance of zeolite catalysts. In terms of xylene isomerization, it is anticipated that a reduction of xylene loss can be achieved by inhibiting the bimolecular transmethylation reactions which should occur mostly at acid sites (especially those on the external surface of the zeolite crystallites) which are stronger than that required for 1,2-methyl group shift.

3.1. Nitrogen and xenon adsorption measurements

For sorption capacity measurements, the data for the modified samples related to the amount of zeolite after modification assuming that the highly dispersed carbonaceous and siliceous deposits do not seriously interfere with sorption data (whereas the deposits have an impact on the specific adsorption of probe molecules for the evaluation of zeolite acidity). As can be seen from the results depicted in Table 1, surface modification by pre-coking or silanization does not exclusively alter the external surface of HZSM-5 and HFER zeolites. Rather, these procedures tend to result in a slight decrease (ca. 10%) in both BET surface area and effective micropore volume compared to the parent zeolite. Therefore, both modification techniques have also an effect on acid sites located in the pore channels of the zeolites. While this was expected for the deposition of carbonaceous residues by pre-coking using methanol as the coke precursor, the formation of small $Si(OH)_x(OC_2H_5)_{4-x}$ species due to hydrolysis reactions is to be assumed in the case of silanization by TEOS.

As also evident from Fig. 1, silanization of HZSM-5 and HFER yields a pore size smaller than its parent zeolite counterpart. Although the calculation method for pore size distribution is not without criticism, it remains a practical method in the micropore region [36]. Nevertheless, water-induced decomposition of TEOS may lead to the formation of small silicon species that can penetrate into the channel systems of ZSM-5 and FER zeolites and thus alters their pore sizes. In contrast, modification by pre-coking hardly affected the pore size distribution of both zeolites. Different locations of carbonaceous and siliceous deposits can be accounted for these findings. It will be shown later that the majority of carbonaceous deposits formed during the combined pre-coking and hydrogen treatment was located on or nearby the outer surface of HZSM-5 and HFER crystallites, while portions of the silica deposits formed during silanization treatment were distributed inside the crystallites. For pre-coking, initial deposition of carbonaceous

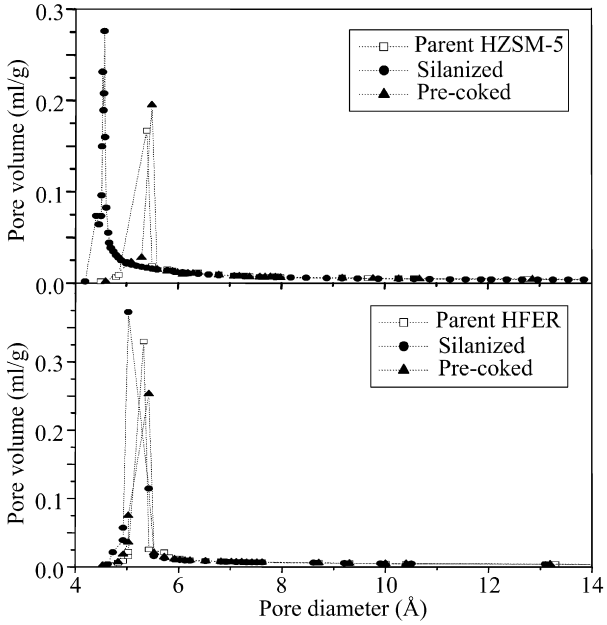

Fig. 1. Variations of Horvath–Kawazoe pore size distribution for HZSM-5 and HFER zeolites before and after surface modification treatments.

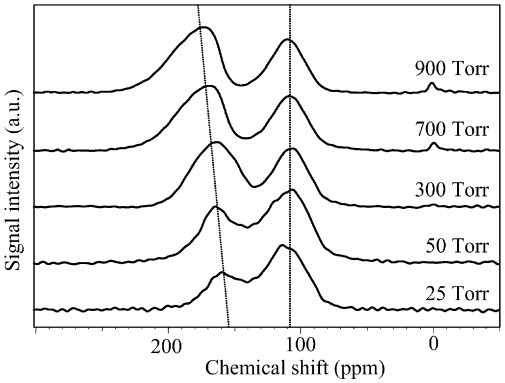

Fig. 2. Room temperature ^{129}Xe NMR spectra of xenon adsorbed on parent HFER sample with various Xe pressures.

residues typically proceeds in HZSM-5 and HFER channels but coke modification by hydrogen treatment at elevated temperatures can result in a transformation and redistribution of the deposits [37,38].

Similar conclusions on pore size variation can be drawn based on the results obtained from room temperature ^{129}Xe NMR of adsorbed xenon. For HZSM-5, which possesses two types of 10-membered ring (10-MR) channels (one zig-zag channel along [100] with dimension ca. 0.51 nm × 0.55 nm and one straight channel along [010] with dimension ca. 0.53 nm × 0.56 nm), all spectra revealed only a single, symmetrical resonance peak whose chemical shift (ranging from 110 to 160 ppm; not shown) increased with increasing Xe loading and revealed a maximal displacement after silanization. On the other hand, HFER zeolite, which possesses 8- and 10-MR channels (dimensions ca. 0.35 nm × 0.48 nm and 0.42 nm × 0.54 nm, respectively), typically gives rise to two overlapping ^{129}Xe NMR resonance peaks (Fig. 2). The peak with higher chemical shift (>160 ppm; lower field), which moves to low

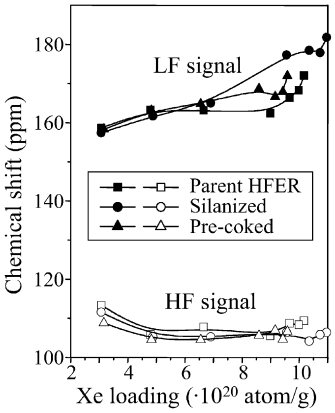

Fig. 3. Variations of ^{129}Xe chemical shift with Xe loading obtained (at 298 K) from HFER zeolite before and after surface modification treatments.

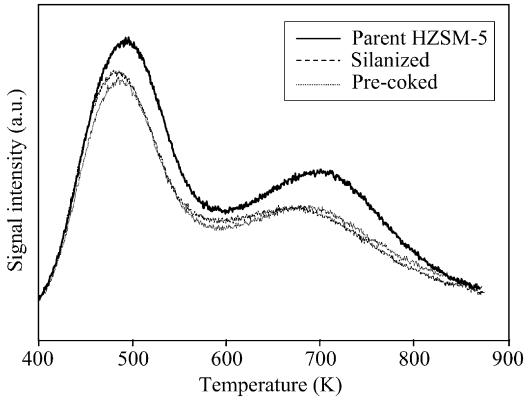

Fig. 4. Ammonia TPD profiles of the parent and modified HZSM-5 samples.

field with increasing Xe loading, can be assigned to xenon in 10-MR channels. On the other hand, the peak at ca. 110 ppm, whose chemical shift is invariant with the Xe loading, arises from Xe in cavities with two opposite 8-MR windows that can accommodate only one Xe atom [39]. As shown in Fig. 2, the relative intensity of the high chemical shift peak increases with Xe pressure. These findings indicate that Xe atoms prefer to adsorb in the 8-MR channels at lower loading. Finally, the signal at 0 ppm appearing at higher Xe loading (>700 Torr) is due to excessive gaseous Xe inside the NMR sample tube.

The effect of surface modification on variations of chemical shift versus Xe density curves can be deduced from Fig. 3. Obviously, only the peak at higher chemical shift reveals an additional increase in a typical upward characteristic of chemical shift versus Xe density following the order: silanized > pre-coked > parent HFER. This can be explained by the decrease in pore volume after sample modification treatments and hence the more extensive Xe–Xe interactions and the resultant increase in the residence time of Xe in the pore channels due to the presence of intracrystalline siliceous or carbonaceous deposits [8].

3.2. Acidity measurements by NH^3-TPD and ^{31}P MAS NMR spectroscopy

Whereas the bulky tributylphosphine oxide (TBPO) molecules having a kinetic diameter of about 0.82 nm cannot enter into the channel systems of HZSM-5 and HFER at room temperature and, thereby, can only be adsorbed on their external surface sites, the smaller-sized ammonia allows the characterization of acid sites in its entirety, i.e., internal and external ones. Fig. 4 shows the NH_3-TPD profiles obtained from parent and modified HZSM-5 samples. The TPD profile is characterized by two broad desorption peaks with maxima at 485 and 700 K assignable to NH_3 desorption from physisorption sites and strong acid sites, respectively. The desorption peaks after modification are located at the same temperature region, i.e., the NH_3-TPD results in Fig. 4 reveal only differences in the number of acid sites but not in their strength due to silanization and pre-coking. Similar findings (not shown) were obtained from the parent and modified HFER samples with desorption peaks at 480 and 725 K. This observation that the strength of acid sites does not change by the surface modifications applied is noteworthy because it is well established that the acidity and pore structure of zeolites are the two important factors determining their activity and selectivity during xylene isomerization [1,2] as well as the skeletal isomerization of 1-butene [40,41].

Due to its voluminous structure, TBPO can merely be adsorbed on acid sites located on the external surface of the crystallites and serves, therefore, as ideal probe molecule for the evaluation of external acidity via solid-state ^{31}P MAS NMR spectroscopy [8,33,35,42]. ^{31}P MAS NMR spectra obtained from the parent and modified HZSM-5 and HFER zeolite samples are shown in Figs. 5 and 6, respectively. Typically, three characteristic ^{31}P NMR resonance peaks at about 90, 72, and 55 ppm were observed for both zeolite sample series. The dashed curves represent results of peak simulation by Gaussian deconvolution method. The signal at 55 ppm can be attributed to the physically adsorbed TBPO, whereas the other two peaks with higher chemical shifts are assigned to chemisorption complexes between TBPO and Brønsted acid sites having different acidic strength [8,33,35,42]. A higher observed chemical shift would represent acid sites with the higher acidic strength. For the characterization and evaluation of external acid sites the ^{31}P NMR peak areas at 90 ppm (strong acid sites) and 72 ppm (moderate/weak acid sites) were taken into account assuming that the amount of TBPO chemisorbed covers all Brønsted acid sites. It should be noted that the signal intensity of physically adsorbed TBPO (55 ppm) represents the excess of TBPO not needed for covering acid sites and depends on the amount of pre-loaded TBPO (see Figs. 5a and 6a).

For both pre-coked zeolite samples, ^{31}P MAS NMR spectra (Figs. 5b and 6b) indicate a significant decrease in the amount of strong surface acid sites (i.e., resonance peak at 90 ppm) compared to their parent counterparts (Figs. 5a and 6a). The integrated peak area decreases from 26 to 3% and 20 to 2% for HZSM-5 and HFER zeolites, respectively. In contrast, marginal reductions in the amount of strong acid sites were found for silanized samples, i.e., from 26 to 21% for HZSM-5 (Fig. 5a vs Fig. 5c) and from 20 to 18% for HFER (Fig. 6a vs Fig. 6c). This implies that silanization by hydrolyzed TEOS is less effective for the passivation of external acidity compared to that

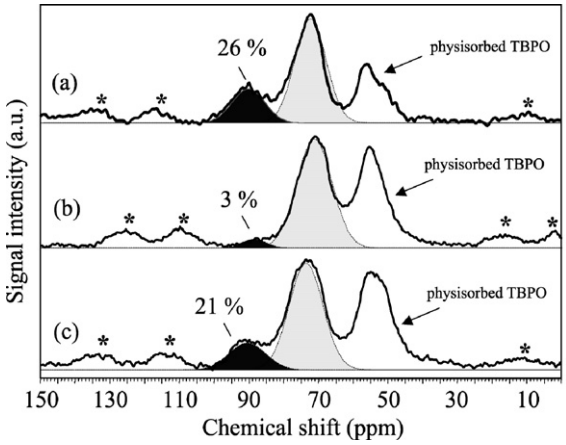

Fig. 5. ^{31}P MAS NMR spectra of TBPO adsorbed on (a) parent, (b) pre-coked, and (c) silanized HZSM-5 samples. The asterisks indicate spinning sidebands.

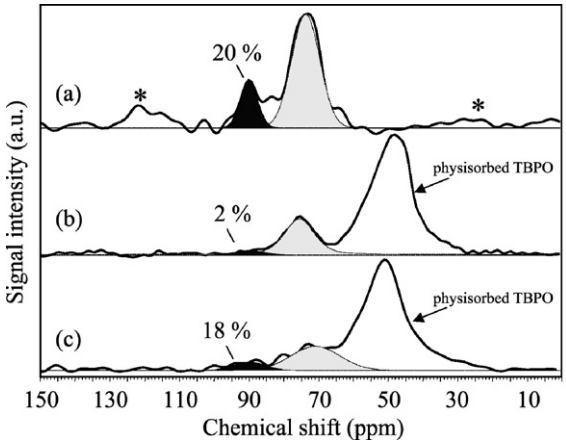

Fig. 6. ^{31}P MAS NMR spectra of TBPO adsorbed on (a) parent, (b) pre-coked, and (c) silanized HFER samples. The asterisks indicate spinning sidebands.

modified by pre-coking treatment. To block all external acid sites via deposition of TEOS it was shown that one needs about 6–10 wt% of SiO_2 [9,43].

3.3. Coke characterization by MALDI-TOF MS

As mentioned earlier, elementary analysis revealed a carbon content of about 0.5 wt% on both pre-coked zeolites. This low amount of carbonaceous deposits makes IR- and NMR-spectroscopic characterization difficult. Temperature-programmed oxidation (TPO) of pre-coked HZSM-5 (Fig. 7) revealed the predominating presence of physisorbed water (weight loss <573 K, which was rather similar to that of the parent zeolite) and only a very small thermogravimetric effect at about 873 K due to coke combustion. This high burning temperature points to hydrogen-deficient, polyaromatic residues [22]. However, these results obtained from TPO studies demand further confirmation. As such, enrichment of carbonaceous residues was accomplished by coke extraction from the dissolved zeolite framework [23].

Carbonaceous residues formed on HZSM-5 during the pre-coking procedure at 723 K and released by HF treatment were

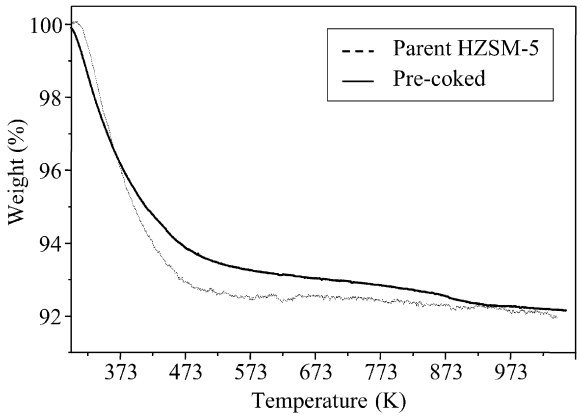

Fig. 7. TPO profiles of the parent and pre-coked HZSM-5 samples.

mainly insoluble in CH_2Cl_2. Therefore, the technique of laser desorption/ionization has been applied for the mass spectrometric characterization of CH_2Cl_2-insoluble coke. The MALDI-TOF mass spectrum revealed a broad molecular weight distribution up to 1300 Da (Fig. 8). Although polyaromatic coke species can be located in the channels of ZSM-5, the findings of nitrogen and xenon sorption as well as the determination of external acidity by ^{31}P MAS NMR spectroscopy suggested that such large carbon entities of $n_C \sim 100$ should preferentially be deposited on the external surface and/or in the pore-mouth region. Starting with a signal at 202 Da, which can be assigned to pyrene ($C_{16}H_{10}$), the mass distribution had a sharp maximum at 363 Da and a second broad maximum at about 750 Da. The complex pattern of the MS signals with repeating mass increments of 24, 37, and 50 Da (Fig. 9) is quite different from that observed for carbonaceous residues formed at lower temperatures ($T < 400$ K) with CH_2 (i.e., 14 Da) increments [29]. Obviously, these building units can be assigned to increments of C_2, C_3H_1, and C_4H_2 entities attached at different positions to a parent polyaromatic structure and resulting in an enlargement of the condensed rings.

The appearance of odd mass signals (e.g., 363 Da) from condensed aromatics is generally attributed either to nitrogen compounds or to fragmentation of oxygen-containing organic compounds. Using methanol as pre-coking material, consequently no nitrogen was observed within the released carbonaceous residues by elementary analysis. Furthermore, severe fragmentation can be excluded using MALDI-TOF mass spectrometry [27]. Therefore, odd mass signals have been attributed to aromatic compounds similar to the structure of phenalene ($C_{13}H_{10}$, molecular weight 166 Da). Phenalene has one CH_2 entity among the aromatic CH groups (see insert of Fig. 10) which can easily split off one of the hydrogen atoms displaying a dominating MS signal at 165 Da [44]. The MS spectrum of phenalene is important for the affirmation that odd mass signals can be attributed to the molecular weight of aromatic hydrocarbons. Thus, the prevailing MS signal at 363 Da has been attributed to a phenalene-like structure of the aromatic compound $C_{29}H_{16}$ (364 Da).

A proposed build-up of polyaromatic carbonaceous deposits on HZSM-5 is shown in Fig. 11. These carbonaceous residues

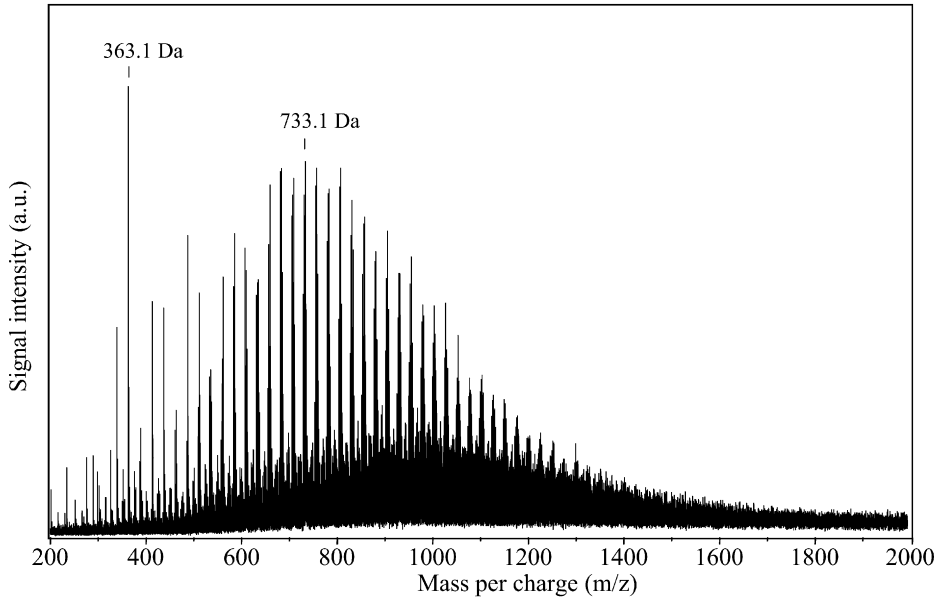

Fig. 8. LDI-TOF mass spectrum of CH_2Cl_2-insoluble coke obtained from HZSM-5 after pre-coking treatment.

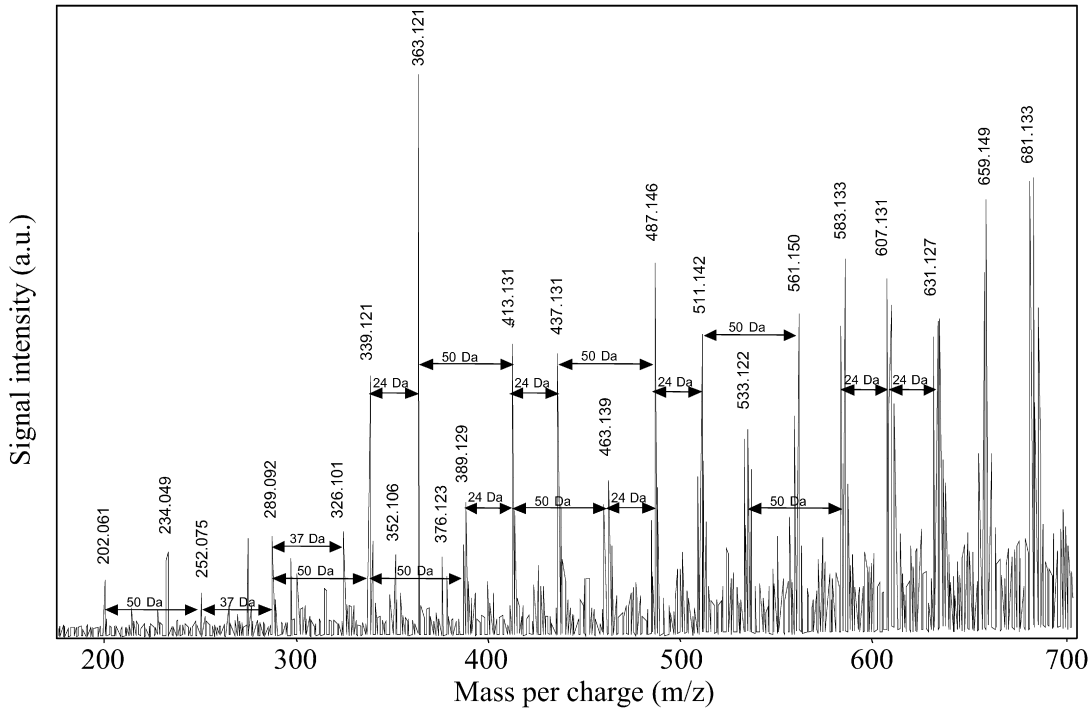

Fig. 9. Low molecular weight part of LDI-TOF mass spectrum of CH_2Cl_2-insoluble coke obtained from HZSM-5 after pre-coking treatment.

have a belt-like topology with a molecular diameter about 0.85 nm. It is proposed that such pyrene-based structures can also be formed inside the channels of ZSM-5 (as shown by Guisnet and Magnoux [23]), migrate to the crystallite surface at higher temperatures ($T > 650$ K) and, finally, passivate efficiently external acid sites (as demonstrated by ^{31}P MAS NMR spectroscopy).

It is noted that more voluminous structures such as coronene ($C_{24}H_{12}$) having a molar mass of 300 Da and a molecular diameter about 1.1 nm have not been observed. Therefore, the formation of belt-like carbonaceous deposits has to be assumed to take place not only within the channels but also in pore-mouth region and on the external surface of HZSM-5 where steric constraints imposed by the zeolite framework do not exist. Finally, some oxygen containing species have also been observed, e.g., MS signals at 234, 266, and 298 Da which can be assigned to pyrene oxygenates.

For the characterization of carbonaceous residues exclusively deposited on the external surface, MALDI/LDI-TOF MS can be performed without dissolving the zeolite. On spent zeo-

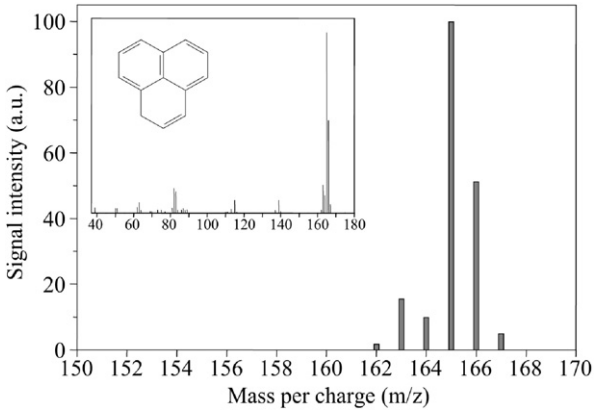

Fig. 10. Upper part of the MS library spectrum of phenalene ($C_{13}H_{10}$) having a molecular weight of 166.22 Da [44] (insert: full spectrum and structure of phenalene).

lite Y-based catalysts used in fluid catalytic cracking, Cerqueira et al. [30] observed coke species with masses up to approximately 400 Da. Even masses dominate the spectrum as well as various series of masses with differences of 14 Da, i.e., CH_2 groups. After HF treatment, the mass distribution extended to about 800 Da and many of the prominent peaks above 400 Da have a corresponding peak with a mass difference of 50 Da, i.e., addition of a C_4H_2 entity to build a new aromatic ring. Furthermore, long series such as those with steps of 14 Da were not observed. Hence, carbonaceous deposits released after dissolving the zeolite Y-based catalyst have been assigned to more polyaromatic hydrocarbons compared to those present on the external surface having partly aliphatic groups. For pre-coked HZSM-5 and HFER (without dissolving the zeolite), LDI-TOF MS spectra revealed coke species with masses up to approximately 900 Da (Fig. 12).

The prominent peaks with repeating mass increments of 190 Da are based on the MS signal of 252 Da which can be assigned to $C_{20}H_{12}$ (see Fig. 11). Within this series up to 822 Da, some adjacent peaks having mass differences of 2 Da were observed, indicating hydrogenation reactions of coke species during H_2 treatment at 773 K. Nevertheless, these peaks are assigned to polyaromatic hydrocarbons. In contrast to the dissolved catalyst, however, the number of coke species was rather limited and they appear to be dissimilar to the proposed belt-like carbonaceous deposits. Therefore, it is concluded that the belt-like coke molecules are located near to the pore openings rather than on the surface of the particles.

3.4. Effect of surface modification of HZSM-5 on selectivity of xylene isomerization

Modern xylene isomerization technologies use *m*-xylene-rich feedstocks of C_8 aromatic cuts containing ethylbenzene (EB). In terms of cost-effective process consideration and to avoid EB accumulation during the recycle loops it is more favorable to dealkylate EB into benzene and ethylene rather than hydroisomerization of EB to xylenes [47].

While enhancement of *para*-selectivity is of great importance for toluene disproportionation [2], the main objective of catalyst modification for the industrial application of xy-

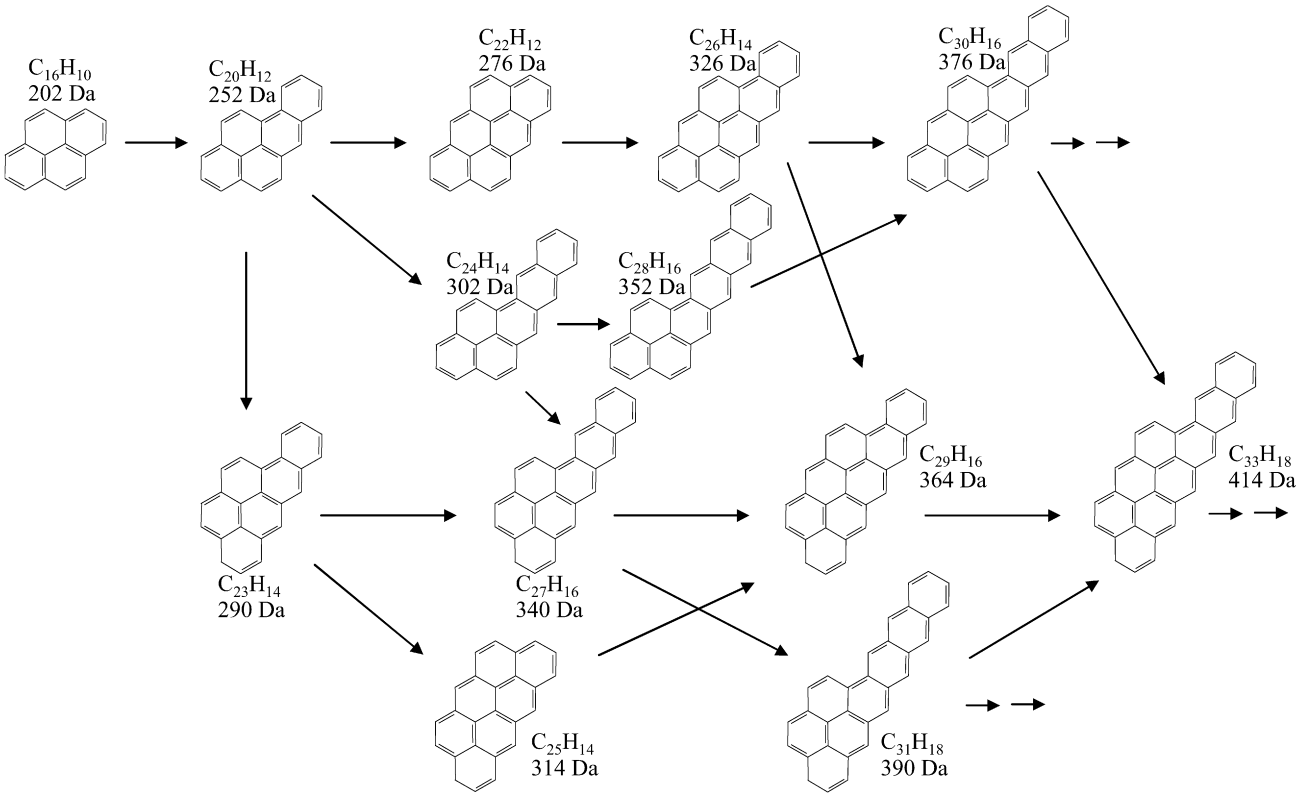

Fig. 11. Schematic illustrations of build-up of polyaromatic deposits formed on HZSM-5.

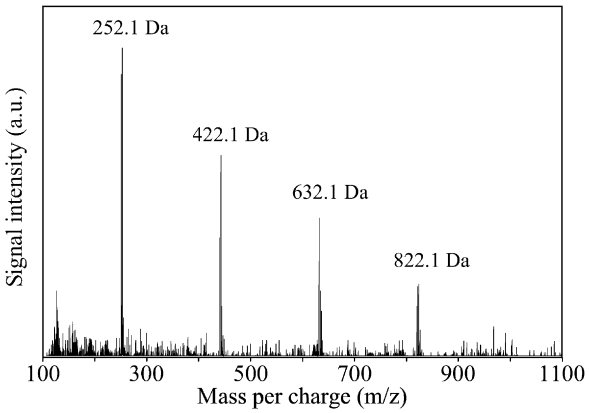

Fig. 12. LDI-TOF mass spectrum of HZSM-5 after pre-coking treatment.

lene isomerization (where the thermodynamic equilibrium distribution of xylene isomers is typically obtained under common operation conditions) is to increase the activity and to reduce the loss of valuable xylenes due to the undesired formation of toluene and trimethylbenzenes (TMBs). On nano-sized HZSM-5 zeolites, an increase of the overall reaction rate can be expected due to the reduction of transport resistance and diffusion path length compared to micro-sized crystallites. However, undesired disproportionation reactions will also be promoted on nano-sized samples due to numerous external acid sites having no steric constraints compared to internal acid sites. Hence, efficient passivation of unselective surface sites on nano-sized HZSM-5 is required to achieve high EB conversion and xylene isomerization rates with low xylene loss.

Such zeolite modifications should be achieved without a markedly increased *para*-selectivity because enhancement of *para*-selectivity is closely connected with the narrowing of pore entrances of the zeolite as well as a decrease in the transport rates and, thereby, affecting the isomerization rate adversely. As a matter of course, contributions to the undesired disproportionation reactions can be expected for xylene conversion on internal acid sites of 10-MR pore size zeolite HZSM-5 where, however, confined pore space interfere the formation of bulky trimethyldiphenylmethane intermediates necessary for xylene disproportionation. Thus it appears that increased shape selectivity for xylene isomerization on nano-sized zeolites stands for decreasing undesired reactions rather than increasing *para*-selectivity.

The transformation of an industrial xylene feed (containing 10 wt% ethylbenzene) revealed an intensive formation of benzene and toluene on the parent and modified HZSM-5 samples (Table 2). Benzene as well as light gases stem certainly from ethylbenzene dealkylation. The paring reaction of methylated aromatics [45] to form short chain olefins and alkanes cannot be excluded but play undoubtedly a minor role. An *m*-xylene conversion of about 30% was chosen to assess the effect of pre-coking and silanization. Obviously, both techniques of surface modification resulted in a decrease of catalyst activity revealed by a longer residence time to obtain a similar degree of conversion such as the parent sample. Comparing the samples at the same conversion level, however, the reduced formation of toluene and TMBs, i.e., a decrease of the xylene loss in the order silanized > parent > pre-coked sample, indicated an increase of shape selectivity by the pre-coking surface modification.

On the other hand, no improvement in *para*-selectivity was observed after the deposition of both coke and silica. Obviously, the 1,2-methyl group shift of xylene isomerization requires less serious reaction conditions compared to EB dealkylation and xylene disproportionation [2]. Therefore, the distribution of xylene isomers obtained on the parent and modified HZSM-5 even at low EB conversion has been near the thermodynamic equilibrium distribution. However, the study of *para*-selectivity during aromatic conversions requires xylene concentrations far from the equilibrium distribution. Therefore, quite different reaction conditions, disregarding the problem of EB conversion, have to be applied to investigate the effect of ZSM-5 modifications on *para*-selectivity during xylene isomerization and are beyond the scope of this study.

The yields of undesirable toluene and TMBs obtained during xylene isomerization at 673 K over the parent and modified HZSM-5 samples are depicted in Fig. 13. Obviously, a reduction of xylene loss can be obtained by zeolite modification either by pre-coking or silanization. However, it is noted that, comparing to the silanized sample with 4 wt% deposited silica, the pre-coking treatment with about 0.5 wt% carbonaceous deposits achieved a far better xylene selectivity. This is mainly due to selective deposition of coke species on the stronger acid

Table 2
Effect of surface modification on xylene transformation over HZSM-5 samples at 673 K and 40 min on stream (in parentheses: distribution of xylene isomers)

	Feed	Parent[a]	Pre-coked[b]	Silanized[b]
m-Xylene conversion (%)		30.7	29.4	30.9
Product yields (wt%)				
Benzene	0.0	7.9	8.9	9.5
Toluene	0.3	13.6	10.4	17.8
Ethylbenzene	10.6	0.6	0.7	0.3
p-Xylene	9.5 (10.7%)	15.8 (21.6%)	14.1 (18.4%)	14.2 (20.5%)
m-Xylene	60.5 (68.3%)	41.9 (57.4%)	42.7 (55.7%)	41.8 (60.4%)
o-Xylene	18.7 (21.0%)	15.3 (21.0%)	19.9 (25.9%)	13.2 (19.1%)
TMBs	0.3	4.0	2.5	3.1
Toluene/TMBs (mol)	1.2	4.5	5.5	7.5

[a] 6 $g_{feed}/(g_{cat}\ h)$.
[b] 4 $g_{feed}/(g_{cat}\ h)$.

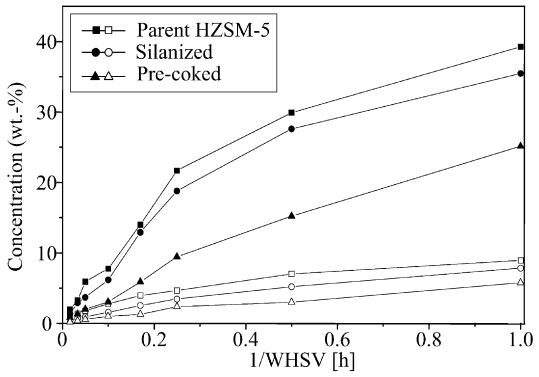

Fig. 13. Effect of contact time (1/WHSV; $g_{feed}/(g_{cat}\,h)$) on formation of toluene (close symbols) and trimethylbenzenes (open symbols) during xylene isomerization over parent, pre-coked and silanized HZSM-5 samples at 673 K.

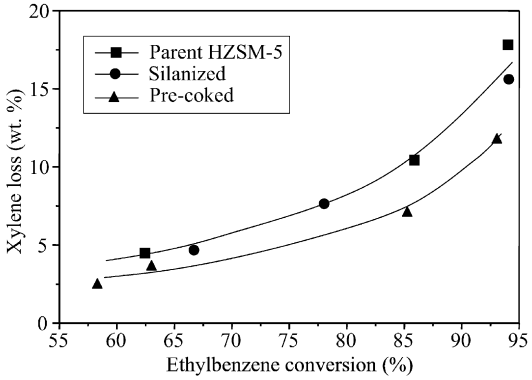

Fig. 14. Effect of surface modification on xylene loss and ethylbenzene conversion during xylene isomerization over parent, pre-coked and silanized HZSM-5 samples at 673 K.

sites on the external surface compared to the deposition of silica, as can be referred from the results obtained from ^{31}P MAS NMR of adsorbed TBPO discussed above.

Moreover, the amount of toluene formed always predominated over the yield of TMBs (in contrast to the assumed equimolar formation of toluene and TMBs). As shown in Table 2, the molecular ratio of toluene/TMBs increased in the order: parent < pre-coked < silanized HZSM-5. Bulky trimethylbenzene molecules (to some extent formed within the zeolite channels and more severely trapped due to channel restrictions after surface modification) are forced to undergo secondary transformation/disproportion into smaller aromatics and polymethylated species. Especially, the aforementioned results obtained from sorption measurements and ^{129}Xe NMR spectroscopy revealed pore narrowing caused by silanization with hydrolyzed TEOS and allow to explain the high toluene/TMBs ratio over the silanized sample in comparison to the parent and pre-coked sample.

On zeolite MCM-22 whose characteristics are between those of large and medium-pore zeolites, Laforge et al. [14] compared different surface modification techniques to enhance the selectivity in *m*-xylene transformation. A similar preferred formation of toluene during xylene transformation has been observed and explained by the strongly limited desorption rate of TMBs. But, neither silanization with hexamethyldisilazane nor pre-coking by *n*-heptane were able to passivate the external hemicages of MCM-22 zeolites. Only poisoning with 2,4-dimethylquinoline was shown to achieve a selective and complete deactivation of external acid sites.

Whereas xylene disproportionation held responsible for toluene and TMBs formation, the conversion of ethylbenzene yielded benzene on the metal-free HZSM-5 samples. As the formation of gaseous olefins as well as tracer studies with ^{14}C-labeled ethylbenzene [46] showed, benzene formation was closely related to the dealkylation of ethylbenzene rather than to the disproportionation of toluene formed. It should be noted that high rates of ethylbenzene dealkylation are requested for the application of industrial xylene feeds to avoid accumulation of ethylbenzene during the recycle loop [47]. To compare the performance of commercial xylene isomerization catalysts, the relationship between the undesired xylene loss and the favored ethylbenzene conversion is an excellent criterion. As visualized in Fig. 14, the loss of xylenes, i.e., the quantity of toluene and TMBs formed, was the lowest on pre-coked HZSM-5 at a given degree of ethylbenzene conversion. Obviously, the pre-coked sample is more effective in ethylbenzene cracking at a low rate of xylene disproportionation. These findings in combination with the aforementioned results obtained from ^{31}P MAS NMR acidity measurements point to the role of external acid sites where disproportionation reactions on nano-sized HZSM-5 take place to a large extent and which can be effectively passivated by pre-coking. The nearly identical behavior of the parent and silanized HZSM-5 sample may be explained by a comparable distribution of external acidic strength. In other words, the bimolecular disproportionation reactions of xylenes predominantly take place on strong acid sites present on the external crystallite surface and/or in the pore-mouth region which remain accessible after the silanization technique applied and which are mainly poisoned after pre-coking.

By pelletizing a HZSM-5 sample (KataLeuna GmbH, Si/Al = 20) with 70 wt% SiO_2 and impregnating with 0.05 wt% Pt, a Pt/HZSM-5 sample has been prepared to improve ethylbenzene conversion and catalyst stability during xylene isomerization [8]. After pre-coking, a substantial reduction in xylene loss was achieved under pilot scale conditions (500 h on stream) while sustaining a desirable activity for ethylbenzene conversion (>55%). On the other hand, modification of the Pt/HZSM-5 sample by liquid deposition of hydrolyzed TEOS resulted in an inefficient passivation of external acidity as indicated by a relatively high xylene loss [32].

In general, multi-cycle chemical vapor/liquid deposition using TEOS under water-free conditions leads to the total inactivation of acid sites on the external surface of HZSM-5 as well as of sites in the pore-mouth region [9,12,13,15,17]. Comparing the effect of silanization (8.5 wt% SiO_2) and pre-coking (5.2 wt% coke) on *para*-selectivity for alkylation of toluene with methanol on HZSM-5, Cejka et al. [7] found that a decrease in the transport rates of xylenes due to the deposition of silica is more decisive for an enhancement of the *para*-selectivity than secondary isomerization reactions on the external surface. Silica deposition via water-induced silanization with TEOS (even substoichiometric amounts of water are suffi-

Table 3
Effect of surface modification on olefin yield during *n*-butene transformation over HFER samples at 573 K and 9 g/(g_{cat} h) (in parentheses: isobutene content within butene fraction)

Yield (wt%)	HFER		
	Parent	Pre-coked	Silanized
C_{1-5} alkanes	0.7	0.7	0.6
Ethylene	0.1	0.1	0.1
Propylene	1.7	1.3	1.4
Butenes	91.3	93.2	93.3
($isoC_4$ content)	(8.4%)	(7.1%)	(3.5%)
Pentenes	1.6	1.2	1.2
C_{6+} compounds	4.6	3.5	3.4
Coke content[a] (g/g_{cat})	8.8	7.5	7.2

[a] After 100 h on stream.

cient) results in a fast, but inefficient passivation of the external acidity as well as in a narrowing and/or blocking of the pore openings as indicated by the relatively high xylene loss and the high toluene/TMBs ratio observed on the one-cycle silanized HZSM-5 sample.

3.5. Effect of surface modification of HFER on skeletal isomerization of n-butene

For *n*-butene isomerization over aged HFER, Guisnet [20] attributed the high isobutene selectivity to the presence of coke species which facilitate the reaction pathway of skeletal isomerization by effectively circumventing the formation of energetically unfavorable intermediates. Therefore, pre-coking of HFER should result in carbonaceous sites catalytically active for the specific formation of isobutene, more or less irrespective on the Si/Al ratio of the zeolite. For comparison, de Menorval et al. [48,49] observed the formation of a thermodynamic equilibrium mixture of propene, butenes, pentenes and carbonaceous species over fresh HFER samples that contain many protonic sites (Si/Al ratio of about 10). Whereas over HFER samples with low Si/Al ratios, the increase in selectivity for isobutene has been attributed to catalyst deactivation by coke formation.

As could be expected for HFER with a low SiO_2/Al_2O_3 ratio of 20, the simultaneous formation of propene, *cis*/*trans*-2-butene, isobutene, and pentenes has been observed on both the parent and modified HFER samples (Table 3). At a reaction temperature of 573 K and WHSV of 9 h^{-1}, the main reaction products were *trans*- and *cis*-butenes although the thermodynamic equilibrium distribution prefers isobutene with about 55% [50]. The low isobutene content obtained at 573 K points to a low isomerization rate over all HFER samples. In particular, silanization of HFER caused a decrease in isobutene formation and can be explained by imposed diffusion restriction due to pore narrowing as indicated by sorption measurements and ^{129}Xe NMR spectroscopy. After the deposition of silica species within the channels, the transport of 'bulky' isobutene molecules should be more hindered compared to the smaller *n*-olefins formed. On the pre-coked sample, no selective formation of isobutene has been observed, i.e., polyaromatic pre-coke deposits do not act as catalytic sites as proposed by the pseudo-

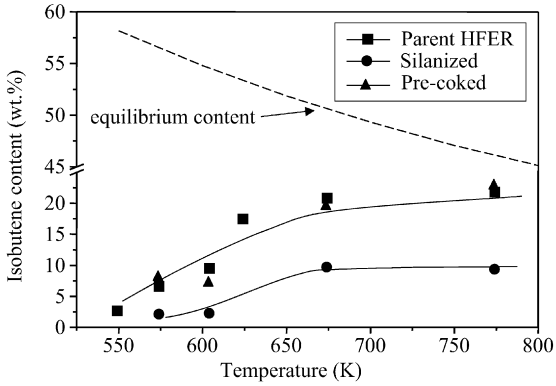

Fig. 15. Effect of reaction temperature on isobutene content during skeletal isomerization of *n*-butene over parent, pre-coked and silanized HFER samples at 9 g/(g_{cat} h).

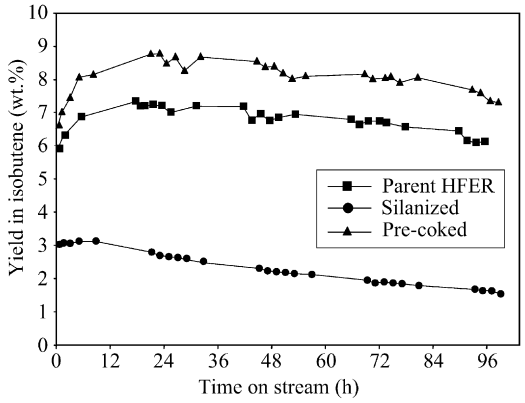

Fig. 16. Effect of time on stream on isobutene yield during skeletal isomerization of *n*-butene over parent, pre-coked and silanized HFER samples at 573 K and 9 g/(g_{cat} h).

monomolecular mechanism. On the contrary, an unexpected high content of longer chain (C_{6+}) hydrocarbons has been observed over parent and modified HFER. These findings point to the dominance of the bi-molecular mechanism which has not been influenced by the surface modification.

Rising the reaction temperature up to 773 K resulted in an increase of the isobutene content over all HFER samples (Fig. 15). Isobutene formation over silanized HFER has still been observed to be the lowest whereas similar isomerization rates were obtained with the parent and pre-coked sample for all reaction temperatures studied. It should be mentioned that (with respect to the temperature dependence of the thermodynamic equilibrium distribution of butenes) the maximal available isobutene content will be the higher the lower the reaction temperature.

Fig. 16 shows the effect of time-on-stream (TOS) on the yield of isobutene for the parent and modified HFER samples at 573 K and WHSV of 9 h^{-1}. Two different shapes of curves are found. With the silanized HFER, a nearly continuous decrease in isobutene formation can be observed. Over parent and pre-coked HFER, an increase in isobutene yield is followed by a decrease. It is noteworthy that the isobutene yield on the pre-coked sample exceeds that on the parent HFER. The increase in isobutene selectivity due to pre-coking is, however, to small

for assigning a specific catalytic activity to these polyaromatic carbonaceous deposits.

After 100 h on stream, the coke content on the pre-coked and silanized HFER are at a similar level of about 7 wt% (Table 2). Therefore, the significant decrease in the selectivity to isobutene with silanization should be explained by the deposition of siliceous materials within the channels and/or at the pore openings rather than by the typical process of catalyst deactivation. On the other hand, the small increase in selectivity to isobutene observed on parent and pre-coked HFER can be attributed to the formation of coke. Obviously, the deposition of carbonaceous residues (up to 9 wt%) during skeletal isomerization of *n*-butene has a minor effect on the diffusion rate of isobutene formed out off the zeolite HFER whereas the deposition of about 4 wt% silica significantly inhibited the diffusivity of isobutene. These findings are in agreement with the aforementioned results from nitrogen and xenon measurements of pore size distribution.

Hence, the product distribution during *n*-butene conversion observed on the parent and modified H-FER samples is controlled by typical zeolite properties such as pore size, density and strength of acid sites. De Menorval et al. [48] have recently put forward such a mechanistic proposal which takes the number of acid sites, i.e., the Si/Al ratio of H-FER, into account.

4. Conclusions

Postsynthetic modification of nano-sized HZSM-5 and HFER zeolites by pre-coking and silanization has been performed to enhance the selectivity of the catalysts maintaining high reaction rates. Detailed features of both surface modification techniques have been obtained by combining the results of catalytic studies with that of zeolite characterization, e.g., N_2 adsorption/desorption measurements, ^{129}Xe NMR spectroscopy, and acid site characterizations by ^{31}P MAS NMR of adsorbed phosphine oxide probe molecules. For HZSM-5 samples pre-coked at 773 K, both MALDI-TOF and LDI-TOF mass spectrometries gave spectra indicating the preferred formation of polyaromatic species in the carbonaceous deposits. Individual coke species with molecular weights up to 1300 Da were obtained to which carbon numbers $n_C \sim 100$ can be assigned. Based on pyrene, a schematic build-up of belt-like carbonaceous residues has been proposed.

For both nano-sized HZSM-5 and HFER zeolites, pre-coking treatment was found to facilitate selective passivation of external acid sites, as evidenced by results from ^{31}P MAS NMR measurements. The decreased proportion of strong surface acid sites on the pre-coked HZSM-5 sample is consistent with the desired reduction of toluene and TMBs formation in the order silanized > parent > pre-coked sample during xylene isomerization. On the contrary, silanization treatments resulted in a nearly unchanged distribution of external acid sites and also led to pore narrowing of both zeolites due to the formation of small siliceous species which can enter in the zeolitic channels. These findings are in agreement with the observed displacement of the toluene/TMBs ratio in favor of toluene in the order silanized > pre-coked > parent HZSM-5 sample pointing to an increase in steric constraints after the modification treatment.

For skeletal isomerization of *n*-butene, the yield of isobutene over parent and pre-coked H-FER samples is similar, i.e., the polyaromatic carbonaceous deposits formed by pre-coking treatment are not catalytically active sites which are claimed to convert selectively *n*-butene into isobutene. Silanization caused a decrease in isobutene formation due to the deposition of siliceous materials within the channels and/or at the pore openings resulting in a reduced diffusivity of isobutene.

Acknowledgments

The support of this work by Deutsche Forschungsgemeinschaft (Germany), National Science Council (Taiwan), and DAAD/NSC Scientific Cooperation program is gratefully acknowledged. F. Bauer expresses his special thanks to Prof. M. Guisnet and Dr. C. Canaff (both University of Poitiers) for stimulating discussions and to Dr. A. Lubentsov (University of Leipzig) for the TPD measurements.

References

[1] J. Cejka, B. Wichterlova, Catal. Rev. Sci. Eng. 44 (2002) 375–421.
[2] T.C. Tsai, S.B. Liu, I. Wang, Appl. Catal. A 181 (1999) 355–398.
[3] M. Guisnet, N.S. Gnep, S. Morin, Microporous Mesoporous Mater. 35–36 (2000) 47–59.
[4] N.Y. Chen, W.W. Kaeding, F.G. Dwyer, J. Am. Chem. Soc. 101 (1979) 6783.
[5] G.J. Nacamuli, R.F. Vogel, WO Patent No. 98 43932 (1998), to Chevron Chemical Company LLC.
[6] W.O. Haag, D.H. Olson, US Patent No. 4 117 026 (1978), to Mobil Oil Corporation.
[7] J. Cejka, N. Zilkova, B. Wichterlova, G. Eder Mirth, J.A. Lercher, Zeolites 17 (1996) 265–271.
[8] F. Bauer, W.H. Chen, Q. Zhao, A. Freyer, S.B. Liu, Microporous Mesoporous Mater. 47 (2001) 67–77.
[9] J.H. Kim, A. Ishida, M. Okajima, M. Niwa, J. Catal. 161 (1996) 387–392.
[10] R. Weber, K. Möller, M. Unger, C. O'Connor, Microporous Mesoporous Mater. 23 (1998) 179–187.
[11] E.F. Vansant, P. Cool, Colloids Surf. A Physicochem. Eng. Aspects 179 (2001) 145–150.
[12] A.B. Halgeri, J. Das, Catal. Today 73 (2002) 65–73.
[13] S.R. Zheng, H.R. Heydenrych, A. Jentys, J.A. Lercher, J. Phys. Chem. B 106 (2002) 9552–9558.
[14] S. Laforge, D. Martin, M. Guisnet, Microporous Mesoporous Mater. 67 (2004) 235–244.
[15] S.R. Zheng, A. Jentys, J.A. Lercher, J. Catal. 241 (2006) 304–311.
[16] D. Van Vu, M. Miyamoto, N. Nishiyama, Y. Egashira, K. Ueyama, J. Catal. 243 (2006) 389–394.
[17] K.Y. Wang, X.S. Wang, G. Li, Catal. Commun. 8 (2007) 324–328.
[18] W.O. Haag, D.H. Olson, P.G. Rodewald, US Patent No. 4 508 836 (1985), to Mobil Oil Corporation.
[19] J.S. Beck, R.A. Crane, M.F. Mathias, J.A. Kowalski, D.N. Lissy, D.L. Stern, WO Patent No. 99 52842 (1999), to Mobil Oil Corporation.
[20] M. Guisnet, J. Mol. Catal. A 182 (2002) 367–382.
[21] W.H. Chen, F. Bauer, E. Bilz, A. Freyer, S.J. Huang, C.S. Lai, S.B. Liu, in: E. van Steen, L.H. Callanan, M. Claeys (Eds.), Recent Advances in the Science and Technology of Zeolites and Related Materials, in: Stud. Surf. Sci. Catal., vol. 154, Elsevier, Amsterdam, 2004, pp. 2269–2274.
[22] F. Bauer, H.G. Karge, in: H.G. Karge, J. Weitkamp (Eds.), Molecular Sieves—Science and Technology, Characterization II, vol. 5, Springer, Berlin, 2006, pp. 249–364.

[23] M. Guisnet, P. Magnoux, Appl. Catal. 54 (1989) 1.
[24] M. Guisnet, P. Magnoux, D. Martin, in: C.H. Bartholomew, G.A. Fuentes (Eds.), Catalyst Deactivation 1997. Proceedings of the 7th International Symposium, October 5–8, Cancun (Mexico), in: Stud. Surf. Sci. Catal., vol. 111, Elsevier, Amsterdam, 1997, p. 1.
[25] F. Bauer, ZfI Mitteilungen Leipzig 156 (1990) 1.
[26] H.S. Cerqueira, P. Ayrault, J. Datka, P. Magnoux, M. Guisnet, J. Catal. 196 (2000) 149–157.
[27] M.W.F. Nielen, Mass Spectrom. Rev. 18 (1999) 309.
[28] S.D. Hanton, Chem. Rev. 101 (2001) 527.
[29] A. Feller, J.O. Barth, A. Guzman, I. Zuazo, J.A. Lercher, J. Catal. 220 (2003) 192–206.
[30] H.S. Cerqueira, C. Sievers, G. Joly, P. Magnoux, J.A. Lercher, Ind. Eng. Chem. Res. 44 (2005) 2069–2077.
[31] C. Sievers, I. Zuazo, A. Guzman, R. Olindo, H. Syska, J.A. Lercher, J. Catal. 246 (2007) 315–324.
[32] F. Bauer, W.H. Chen, H. Ernst, S.J. Huang, A. Freyer, S.B. Liu, Microporous Mesoporous Mater. 72 (2004) 81–89.
[33] W.H. Chen, T.C. Tsai, S.J. Jong, Q. Zhao, C.T. Tsai, I. Wang, H.K. Lee, S.B. Liu, J. Mol. Catal. A 181 (2002) 41–55.
[34] A.R. Pradhan, T.S. Lin, W.H. Chen, S.J. Jong, J.F. Wu, K.J. Chao, S.B. Liu, J. Catal. 184 (1999) 29.
[35] Q. Zhao, W.H. Chen, S.J. Huang, S.B. Liu, in: M. Anpo, M. Onaka, H. Yamashita (Eds.), Science and Technology in Catalysis, in: Stud. Surf. Sci. Catal., vol. 145, Elsevier, Amsterdam, 2003, pp. 205–209.
[36] G. Horvath, K. Kawazoe, Chem. Eng. Jpn. 16 (1983) 470.
[37] F. Bauer, H. Ernst, E. Geidel, R. Schodel, J. Catal. 164 (1996) 146–151.
[38] L.Y. Fang, S.B. Liu, I. Wang, J. Catal. 185 (1999) 33.
[39] M.A. Springuel-Huet, A. Nossov, F. Guenneau, V. Fornes, A. Corma, J. Fraissard, A. Gedeon, in: E. van Steen, L.H. Callanan, M. Claeys (Eds.), Recent Advances in the Science and Technology of Zeolites and Related Materials, in: Stud. Surf. Sci. Catal., vol. 154, Elsevier, Amsterdam, 2004, pp. 1204–1211.
[40] P. Meriaudeau, C. Naccache, Adv. Catal. 44 (2000) 505–543.
[41] S. van Donk, J.H. Bitter, K.P. de Jong, Appl. Catal. A 212 (2001) 97–116.
[42] Q. Zhao, W.H. Chen, S.J. Huang, Y.C. Wu, H.K. Lee, S.B. Liu, J. Phys. Chem. B 106 (2002) 4462–4469.
[43] B. Wichterlova, J. Cejka, Catal. Lett. 16 (1992) 421–429.
[44] S.E.d.N.M.S.D.C. Stein, in: P.J. Linstrom, W.G. Mallard (Eds.), NIST Chemistry WebBook, NIST Standard Reference Database Number 69, National Institute of Standards and Technology, Gaithersburg, MD, 2005, http://webbook.nist.gov.
[45] R.F. Sullivan, R.P. Sieg, G.E. Langlois, C.J. Egan, J. Am. Chem. Soc. 83 (1961) 1156.
[46] F. Bauer, E. Bilz, A. Freyer, Appl. Catal. A 289 (2005) 2–9.
[47] H.H. John, H.D. Neubauer, P. Birke, Catal. Today 49 (1999) 211–220.
[48] B. de Menorval, P. Ayrault, N.S. Gnep, M. Guisnet, J. Catal. 230 (2005) 38–51.
[49] B. de Menorval, P. Ayrault, N.S. Gnep, M. Guisnet, Appl. Catal. A 304 (2006) 1–13.
[50] D.R. Stull, E.F.J. Westrum, G.C. Sinke, The Chemical Thermodynamics of Organic Compounds, Wiley & Sons, New York, 1969.